Quasiparticle self-consistent GW calculation of Sr_2RuO_4 and $SrRuO_3$

Siheon Ryee,[1] Seung Woo Jang,[1] Hiori Kino,[2] Takao Kotani,[3] and Myung Joon Han[1,4,*]

[1]*Department of Physics, Korea Advanced Institute of Science and Technology (KAIST), Daejeon 305-701, Korea*

[2]*National Institute for Materials Science, Sengen 1-2-1, Tsukuba, Ibaraki 305-0047, Japan*

[3]*Department of Applied Mathematics and Physics, Tottori University, Tottori 680-8552, Japan*

[4]*KAIST Institute for the NanoCentury, Korea Advanced Institute of Science and Technology, Daejeon 305-701, Korea*

(Received 30 July 2015; revised manuscript received 22 January 2016; published 11 February 2016)

By using quasiparticle self-consistent GW calculations, we reexamined the electronic structure of Sr_2RuO_4 and $SrRuO_3$. Our calculations show that the correlation effects beyond the conventional local density approximation and generalized gradient approximation are reasonably well captured by the QSGW self-energy without any *ad hoc* parameter or any ambiguity related to the double-counting and the downfolding issues. While spectral weight transfer to the lower and upper Hubbard band is not observed, the noticeable bandwidth reduction and effective-mass enhancement are obtained. Important features in the electronic structures that have been debated over the last decades such as the photoemission spectra at around -3 eV in Sr_2RuO_4 and the half-metallicity for $SrRuO_3$ are discussed in the light of our QSGW results and in comparison with the previous studies. The promising aspects of QSGW are highlighted as a first-principles calculation method to describe the moderately correlated $4d$ transition-metal oxides along with the limitations of QSGW.

DOI: 10.1103/PhysRevB.93.075125

I. INTRODUCTION

Since the seminal discovery of unconventional superconductivity at $\leqslant 1$ K, Sr_2RuO_4 (SRO214) has been studied extensively [1]. The crystal structure of SRO214 is of the K_2NiF_4 type at low temperature, as shown in Fig. 1, and its normal phase is a paramagnetic metal. Its intriguing electronic behavior and superconductivity are still a subject of active study [2–9]. $SrRuO_3$ (SRO113) is a ferromagnetic metal with a transition temperature $T_c \sim 160$ K. The observed magnetic moment is $\mu = 1.1\mu_B$–$1.7\mu_B$ f.u.$^{-1}$ [10–14] and the stable structure at low temperature is an orthorhombic perovskite with a $GdFeO_3$-type distortion. The electronic structure of SRO113 is located near the half-metallicity, as reported by density functional theory (DFT) + U calculations [15–17]. The thin film SRO113 is of particular interest as a widely used bottom electrode [18–20] and is intensively studied for the possibility of a new field-effect device [21–23].

Considering their fundamental and technological importance, it is essential to understand correctly the electronic structures of SRO214 and SRO113. For SRO214, the early electronic structure calculations [24–29] showed that the states near the Fermi level (E_F) consist of antibonding combinations of Ru t_{2g} and O $2p$, and the Fermi surface is composed of the Γ-centered electron-like sheets (called β and γ) and the X-point-centered hole-like sheet (called α) [24–29]. The local density approximation (LDA) Fermi-surface topology was in good agreement with that of de Haas–van Alphen (dHvA) experiments [30,31], but does not seem to be with the results of angle-resolved photoemission spectroscopy (ARPES) [32,33] in the sense that one-electron-like (β) and two-hole-like (α and γ) Fermi surfaces were observed by ARPES [32,33]. However, it later turned out to be a surface effect [34–36]. Therefore, the overall features of the electronic structure can be regarded as being well described by the conventional electronic structure calculation techniques such as the LDA and the generalized gradient approximation (GGA).

However, the details of the electronic structure are still not clearly understood. A series of recent studies that identify SRO214 as a "Hund metal" [2–4] can be one example showing that the previous understanding based on the conventional electronic structure calculations was not enough. Also, there was a debate regarding the detailed feature of electronic levels at ~ -3 eV revealed by x-ray photoemission spectroscopy (XPS) [37–42]. According to XPS and resonant XPS, the indication of the lower Hubbard band (LHB) of Ru $4d$ states is observed while the LDA calculation predicts that those features should be attributed mainly to the oxygen states [37]. The experimental effective mass ($m^*/m_{\mathrm{LDA}} \simeq 2$–$5$) is also significantly larger than the LDA value [30,43–45]. While dynamical mean-field theory (DMFT) can be a reasonable alternative in this situation [2,42,46–48], its parameter dependency has caused discrepancy even among the DMFT results. For example, the calculations by Pchelkina *et al.* [48] and by Liebsch *et al.* [47] seem to give different answers to the nature of the states at ~ -3 eV most likely due to their different choices of U and J. Beside the ambiguity in the double-counting term in DFT + DMFT, this parameter dependency is a well-known problem for the first-principles description of correlated electron systems. It is also noted that another well-established technique, DFT + U, is not useful for paramagnetic SRO214 because of its Hartree–Fock nature which always prefers the magnetic solution [49].

For SRO113 the situation is similar to that of SRO214; although the overall features can be described by conventional methods, the details are not clearly understood. Note that DFT + U can be used for this case as the ground state of SRO113, which is (ferro) magnetic. For the bulk phase, the LDA, LDA + U, and self-interaction correction (SIC) give the correct ferromagnetic solution although the calculated moment shows some deviations [15,50–52]. For the thin film SRO113, however, the experimentally observed metal-to-insulator transition (MIT) and the ferromagnetic-to-nonmagnetic transition

*mj.han@kaist.ac.kr

as a function of layer thickness are not consistently reproduced by these techniques [17,53–57]. For example, the single-layer SRO113 is predicted to be either ferromagnetic or nonmagnetic depending on the choice of the exchange-correlation functional and the U values [53,55–57]. As in the case of SRO214, DMFT has made important contributions for SRO113 [3,4,58,59], but it is still not completely satisfactory because of the limitations, such as the parameter dependency. Also, the details of the spectroscopic data of SRO113 need further clarifications [60–64].

In this paper, we re-investigate the electronic structure of these two classical 4d transition-metal-oxide systems by using the quasiparticle self-consistent GW (QSGW) [65–67] method. To the best of our knowledge, this well-established calculation technique has never been applied to the ruthenates, while the GW self-energy can be expected to give a good description of metallic and weakly correlated systems. Despite its limitation to take the Hubbard-like on-site Coulomb interactions into account, QSGW has a distinctive advantage as a fully self-consistent "parameter-free" technique. Due to the recent experimental progress in making "complex oxide" structures such as thin films and hetero-interfaces, the parameter-free description of correlated systems has become more imperative. In this context, the QSGW study of these classical 4d systems can be of significant importance, and its ability and limitation should be carefully investigated.

Our calculations show that the effect of electronic correlations beyond LDA and GGA is reasonably well captured by the QSGW procedure, and a noticeable bandwidth reduction is observed. For the paramagnetic SRO214, the effect of GW self-energy is clearly distinctive from the other many-body calculation (e.g., DMFT) in that the spectral weight transfer and the LHB feature do not appear in the QSGW result. For the ferromagnetic SRO113, the QSGW band structure is quite similar to the results of DFT + U and the half-metallic band structure is reproduced.

II. COMPUTATION METHOD

A. Quasiparticle self-consistent GW method

In the QSGW method, the self-energy $\Sigma(\mathbf{r},\mathbf{r}',\omega)$ is calculated within the GW approximation, and H_0 (the noninteracting Hamiltonian describing quasiparticles or band structures) and W [dynamically screened Coulomb interactions between quasiparticles within the random-phase approximation (RPA)] is updated self-consistently [65–68]. The static nonlocal one-particle exchange-correlation potential $V^{\mathrm{xc}}(\mathbf{r},\mathbf{r}')$ is generated from $\Sigma(\mathbf{r},\mathbf{r}',\omega)$ as

$$V^{\mathrm{xc}} = \frac{1}{2}\int_{-\infty}^{\infty} d\omega \mathrm{Re}[\Sigma(\omega)]\delta(\omega - H^0) + \mathrm{c.c.}$$
$$= \sum_{ij} |\psi_i\rangle\langle\psi_i| \frac{\mathrm{Re}[\Sigma(\varepsilon_i) + \Sigma(\varepsilon_j)]}{2} |\psi_j\rangle\langle\psi_j|,$$

where ε_i and $|\psi_i\rangle$ refer to the eigenvalues and eigenfunctions of H_0, respectively, and $\mathrm{Re}[\Sigma(\varepsilon)]$ is the Hermitian part of the self-energy [65,66]. With this V^{xc}, one can solve a new static one-body Hamiltonian H_0 and continue to apply the GW approximation until self-consistency is achieved. The distinctive feature of QSGW compared with DFT + U and DMFT is that it does not require any *ad hoc* parameters. Previous studies, ranging from atoms [69], semiconductors [66,67,70,71], to the various 3d transition-metal oxides [66,67,72–74] and 4f electron systems [75] have demonstrated its capacity to investigate many different types of correlated materials.

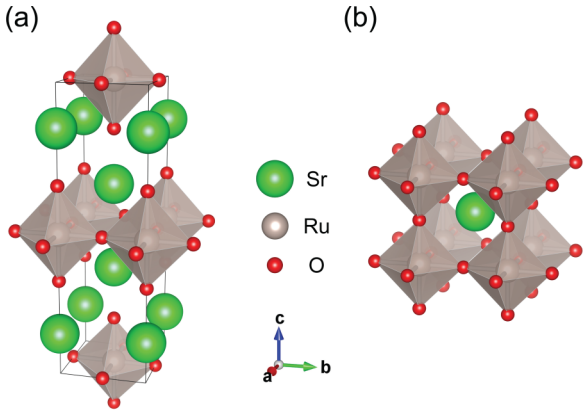

FIG. 1. The crystal structure of (a) SRO214 and (b) SRO113. The green, gray (octahedra), and red spheres represent Sr, Ru (RuO_6 cage), and O atoms, respectively.

B. Computation details

Our implementation of QSGW in ECALJ code [76] is based on the "augmented plane wave (APW) + muffin-tin orbital (MTO)" method, designated by "PMT" [77]. The accuracy of this scheme was proven to be satisfactory [77]. A key feature of this scheme for QSGW is that the expansion of V^{xc} can be made with MTOs, not APWs, which enables us to make the real-space representation of V^{xc} at any $\mathbf{k}$ point. In contrast to the previous approach based on full potential linearized muffin-tin orbital (FP-LMTO) [67], our scheme is free from the fine tuning of MTO parameters.

We used the in-plane and out-of-plane lattice constant of 3.87 and 12.73 Å, respectively, for the body-centered tetragonal SRO214. For SRO113, the cubic perovskite structure is considered as shown in Fig. 1(b). The pseudocubic lattice constant of the orthorhombic structure is 3.93 Å [78]. We used $6 \times 6 \times 6$ [79] and $8 \times 8 \times 8$ $\mathbf{k}$ points for the self-energy calculation in the first Brillouin zone of SRO214 and SRO113, respectively. For cubic SRO113 we also performed DFT + U calculations using the OPENMX code [80] to make a comparison with previous studies. Both the LDA [81] and GGA [82] functionals were used in combination with the Dudarev form of DFT + U [83,84]. $16 \times 16 \times 16$ $\mathbf{k}$ points were adopted for DFT + U calculations.

III. RESULT AND DISCUSSION

A. Electronic structure of Sr_2RuO_4

Our LDA result is in good agreement with the previous calculations [24–29], see Figs. 2 (black dotted lines) and 3. The Van Hove singularity (VHS) is located at ~60 meV above the E_F and the density of states (DOS) at E_F is $N(E_F) \simeq 3.34$ states/(eV f.u.). The Ru t_{2g} state is dominant near E_F and is hybridized with O 2p. From Figs. 2(a), 2(c), and 2(d), one can

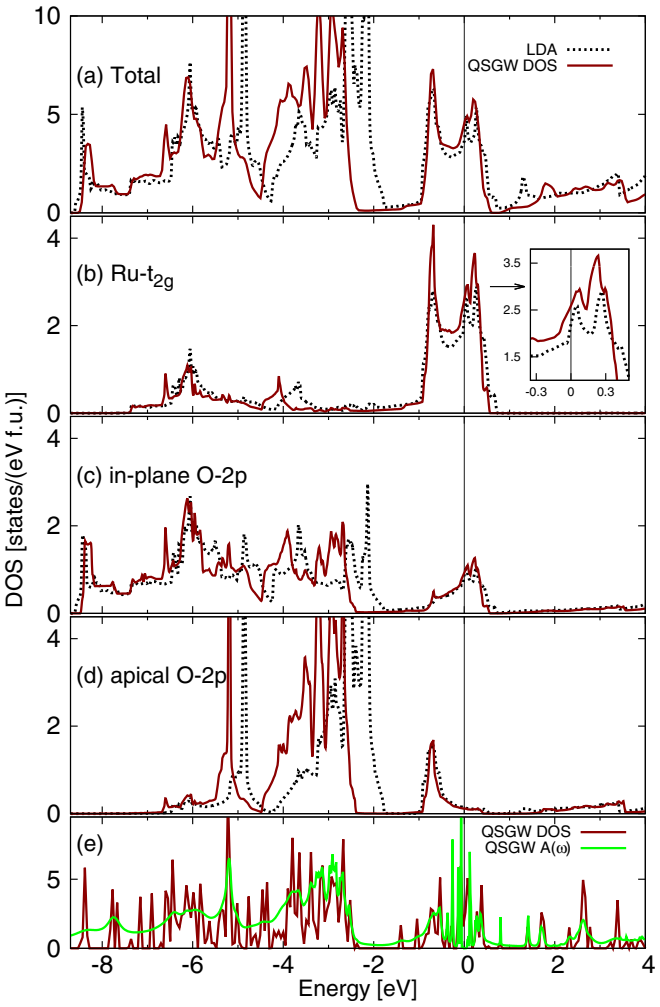

FIG. 2. The calculated (a) total DOS and (b)–(d) PDOS for SRO214 by LDA (black dotted lines) and QSGW (red solid lines). The spectral function $A(\omega)$ calculated by QSGW self-energy is plotted in panel (e) (green solid line) along with the noninterpolated total DOS (red solid line). The Fermi level is set to zero.

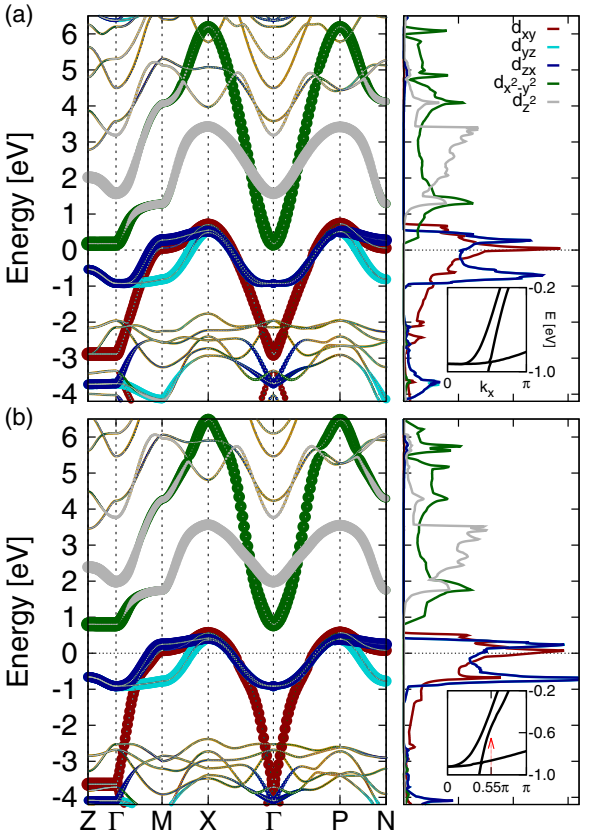

FIG. 3. The calculated band dispersion and the Ru d PDOS for SRO214 by (a) LDA and (b) QSGW. The red, cyan, blue, green, and gray lines refer to the Ru d_{xy}, d_{yz}, d_{zx}, $d_{x^2-y^2}$, and d_{z^2} states, respectively. The yellow lines represent the O and Sr states (not shown in the DOS). The thickness of the bands corresponds to the amount of the corresponding orbital character. The red and blue arrows represent the bandwidth of each band. The Fermi level is set to zero. The insets highlight the band dispersion around -0.6 eV along Γ to M $(\pi,0,0)$ by (a) the LDA and (b) QSGW. A sudden change of slope at $(0.55\pi,0,0)$ is observed only in QSGW (red arrow). This feature is reflected in the PDOS [see Fig. 4(b)].

see that the total DOS in the range of -4 to -2 eV is largely attributed to the apical O $2p$. The calculated band dispersion is presented in Fig. 3(a). The bandwidth of the two-dimension-like (2D-like) d_{xy} state is about two times larger than that of $d_{yz,zx}$ states. The nonbonding O $2p$ state is located within -4 to -2 eV as can also be seen in Fig. 2(d).

The QSGW DOS is presented in Fig. 2 (red solid lines) [85]. While the overall shape of the DOS is not much different from the LDA results, some differences are observed. The two VHS located at $\sim+60$ and $\sim+260$ meV in the LDA [24–29] become closer in QSGW, shifting to $\sim+70$ and $\sim+220$ meV, respectively [see inset in Fig. 2(b)]. Both the bonding (at ~-6 eV) and the antibonding (around E_F) part of Ru $4d$ states becomes flatter in their dispersion compared with the LDA result. The t_{2g} bandwidth is slightly reduced (see Figs. 2 and 3). An interesting feature is found in the d_{xy} band dispersion along Γ to M. The different dispersion at ~-0.6 eV (see Fig. 3 insets) is related to the more pronounced peak in the QSGW partial density of states [PDOS; see Fig. 4(b)]. The O $2p$ states are shifted to the lower-energy regions in QSGW [Figs. 2(c)–2(d)]. The Sr $4d$ state is further pushed up to ∼4 eV (not shown).

The further details of the Ru t_{2g} state are of particular interest because the LHB feature at around -3 eV has been a subject of debate [37–39,42,47,48]. Figure 4 compares the PDOS calculated by the LDA, LDA + DMFT, and QSGW. Note that the states in the range of -4 to -1 eV are noticeably larger in the LDA + DMFT than in the LDA and QSGW especially for $d_{yz,zx}$. It is related to the spectral weight transfer from the near-E_F regions to the LHB. This is one of the main features of DMFT calculations and was the main point of the previous debate between the LDA, DMFT [37,38,48], and the XPS experiment [39], while the QSGW result in this region is similar to the LDA rather than to DMFT. Namely, the QSGW procedure does not capture the dynamic "Mott–Hubbard physics" while it still takes some correlation effect into account, as reflected in the bandwidth reduction and the mass enhancement. This can also be seen in Fig. 5(a). One

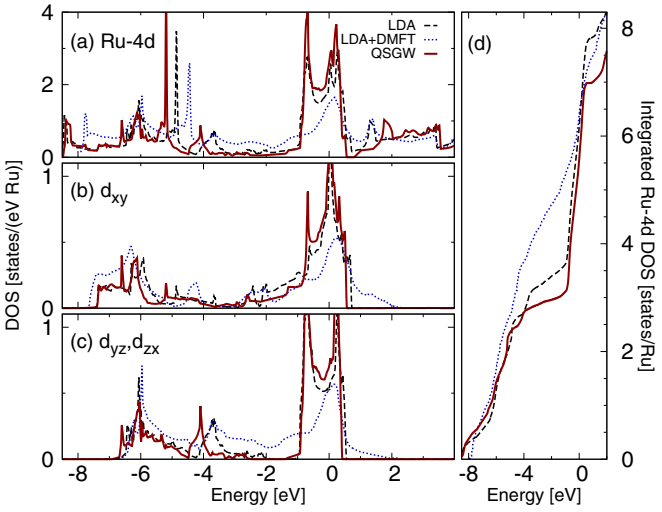

FIG. 4. (a)–(c) The PDOS for SRO214 calculated by the LDA (black dashed lines), LDA + DMFT [48] (blue dotted lines) and QSGW (red solid lines). The e_g states in the previous LDA and DMFT study were identical [48] and are not shown here. (d) The integrated d DOS defined as $N(E) = \int_{-\infty}^{E} n(\varepsilon)d\varepsilon$, where $n(\varepsilon)$ is the DOS at energy ε. Each value was normalized to have an equal number of states at $E = \infty$. E_F is set to zero.

can notice the shoulder-like LHB feature in the XPS spectrum at ~ -3 eV being consistent with the LDA + DMFT, while both the LDA and QSGW give less states in this energy region. The theoretical spectra in Fig. 5(a) were broadened as in Ref. [48]. Not surprisingly, this LHB feature of DMFT is more pronounced in $d_{yz,zx}$ states than in d_{xy} states because of the narrower bandwidth. This point is highlighted in the integrated DOS [Fig. 4(d)]. While the total number of Ru states (the integrated value up to E_F) is basically the same in all three calculations, the DMFT value gets increased over a wider energy range. On the other hand, the LDA and QSGW values are much more rapidly increased in the narrower energy range of $-0.5 \leqslant \varepsilon \leqslant 0$ eV. Since the QSGW bandwidth is narrower than that of the LDA, this increase is more pronounced in

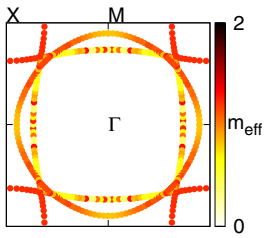

FIG. 6. The Fermi surface of SRO214 at $k_z = 0$ plane. The color represents the calculated effective mass defined as $m_{\mathrm{QSGW}}/m_{\mathrm{LDA}}$.

QSGW. Our result demonstrates the characteristic feature of QSGW to take into account of electron correlations distinctive from DMFT, especially regarding the incoherent states at -3 eV.

The Ru e_g bands are also affected by the QSGW self-energy (see Fig. 3). The slight upshift of the e_g antibonding bands is consistent with the previous study of $SrVO_3$ [86]. As a result, the $d_{x^2-y^2}$ band does not touch E_F even at the Γ and Z points (see Fig. 3). The O $2p$ nonbonding state is located at -3.5 to -2.5 eV in QSGW (Fig. 3), which is in better agreement with the recent ARPES result [87] than the LDA.

The overall shape of the Fermi surface calculated by QSGW (see Fig. 6) is consistent with the LDA [24–29], dHvA [30,31], and ARPES [34–36]. The inclusion of spin-orbit coupling as a perturbative correction within QSGW induces relatively small modifications at the band crossing points (not shown) [89]. The calculated effective mass at each **k** direction is shown in Fig. 6 with a color plot where m^*/m_{LDA} is estimated simply by taking the derivative of band dispersions. Along the Γ to X $(\pi,\pi,0)$ line, the mass enhancement by QSGW is about 15% ($m^*_{xy}/m_{\mathrm{LDA}} \simeq 1.15$) for d_{xy} and 22% ($m^*_{yz,zx}/m_{\mathrm{LDA}} \simeq 1.22$) for $d_{yz,zx}$, respectively. For the Γ to M $(\pi,0,0)$ line, $m^*_{xy}/m_{\mathrm{LDA}} \simeq 0.83$ and $m^*_{yz,zx}/m_{\mathrm{LDA}} \simeq 0.78$.

It is instructive to compare the QSGW result with the DMFT calculations and experiments while the DMFT effective mass strongly depends on the U and J values. The value reported by Mravlje *et al.* with $U = 1.7$ and $J = 0.0$ to 0.1 eV is $m^*/m_{\mathrm{LDA}} \simeq 1.7$ for both d_{xy} and $d_{yz,zx}$ [2]. This value is

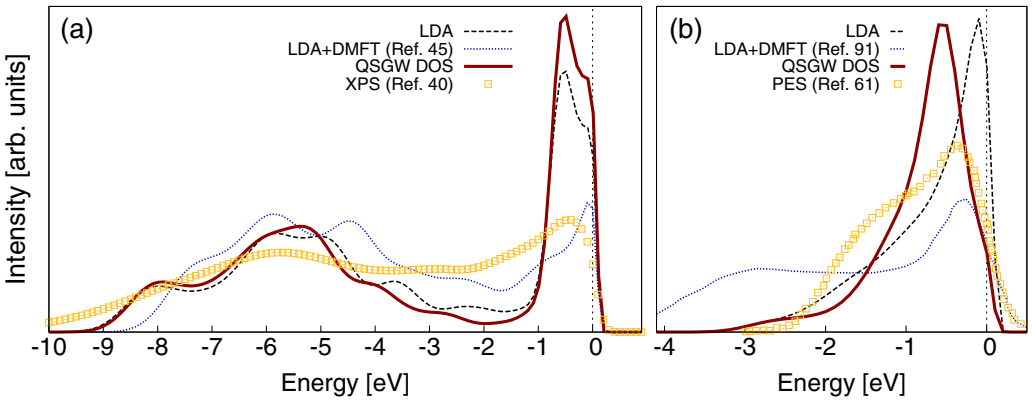

FIG. 5. The experimental and calculated spectra of (a) SRO214 and (b) Ru 4d states of SRO113. Panel (a) shows the XPS spectrum (yellow dots) by Yokoya *et al.* [39] plotted along with the Gaussian-broadened DOS by the LDA (black dashed line), LDA + DMFT (blue dotted line) [48], and QSGW (red solid line). Panel (b) shows the PES spectrum (yellow dots) by Takizawa *et al.* [64] obtained from orthorhombic SRO113 at room temperature and plotted with the Gaussian-broadened DOS of cubic SRO113 (LDA and QSGW) and the orthorhombic SRO113 (LDA + DMFT [88]). Only Ru 4d states are plotted in panel (b). The intensities were normalized in the area under curves.

significantly smaller than that obtained by the other DMFT calculations, e.g., by Pchelkina *et al.*, $m^*/m_{\rm LDA} \simeq 2.6$ and 2.3 for d_{xy} and $d_{yz,zx}$, respectively (with $U = 3.1$ and $J = 0.7$ eV obtained from the constrained LDA) [48], and by the same group but with $U = 2.3$ and $J = 0.2$ eV, $m^*/m_{\rm LDA}$ is $\simeq$2.3 and 2.0 for d_{xy} and $d_{yz,zx}$, respectively [2]. These DMFT values were calculated from $m_{\rm DMFT}/m_{\rm LDA} \equiv Z^{-1}_{\rm DMFT} = [1 - \partial_\omega {\rm Re}\Sigma_{\rm DMFT}(\omega)]_{\omega=0}$. Our estimate from the QSGW self-energy yields $Z^{-1}_{\rm QSGW} \simeq 1.82$ for d_{xy} and 1.71 for $d_{yz,zx}$ [90], which is not much different from the DMFT values of 1.7 calculated by Mravlje *et al.* with $U = 1.7$ and $J = 0.0$ to 0.1 eV [2]. Note that $U = 2.3$ and $J = 0.4$ eV were suggested to be reasonable [2] in comparison to dHvA measurements [30,43], and that the experimental values are larger than the QSGW. The early ARPES reports $m^*/m_{\rm LDA} \simeq 2.5$ [45] and the more recent measurement by Iwasawa *et al.* is $m^*_{xy}/m_{\rm LDA} \simeq 3.7$ and $m^*_{yz,zx}/m_{\rm LDA} \simeq 2.0$ [87]. There are two reports from the dHvA experiment; $m^*_{xy}/m_{\rm LDA} \simeq 4.1$ and $m^*_{yz,zx}/m_{\rm LDA} \simeq 3.3$ by Mackenzie *et al.* [30], and $m^*_{xy}/m_{\rm LDA} \simeq 5.5$ and $m^*_{yz,zx}/m_{\rm LDA} \simeq 3.4$ by Bergemann *et al.* [43].

B. Electronic structure of cubic $SrRuO_3$

The LDA result for cubic SRO113 is in good agreement with previous studies [15,50–52] (see Figs. 7 and 8). The calculated magnetic moment of $\mu = 1.28\mu_{\rm B}$/f.u. also agrees reasonably well with the literature values of $\mu = 1.09\mu_{\rm B}$/f.u. (calculated by VASP) and $\mu = 1.26\mu_{\rm B}$/f.u. (calculated by SIESTA) [15]. The Sr $4d$ state is located above $\sim$4 eV (not shown) and the nonbonding state of O $2p$ is within -4 to -2 eV. The antibonding Ru t_{2g} character dominates the near-E_F region and the bonding complex is located at -8 to -4 eV. A clear splitting between the up- and down-spin DOS is noticed and is responsible for the ferromagnetism in this material. The effect of orthorhombic distortion (not taken into account in our calculation) has been investigated previously. For example, Rondinelli *et al.* [15] showed that the result from orthorhombic structure is similar to the cubic case other than the slightly reduced exchange splitting at the Γ point and the bandwidth reduction by $\sim$0.35 eV for t_{2g}, 1.5 eV for e_g, and 0.6 eV for O $2p$.

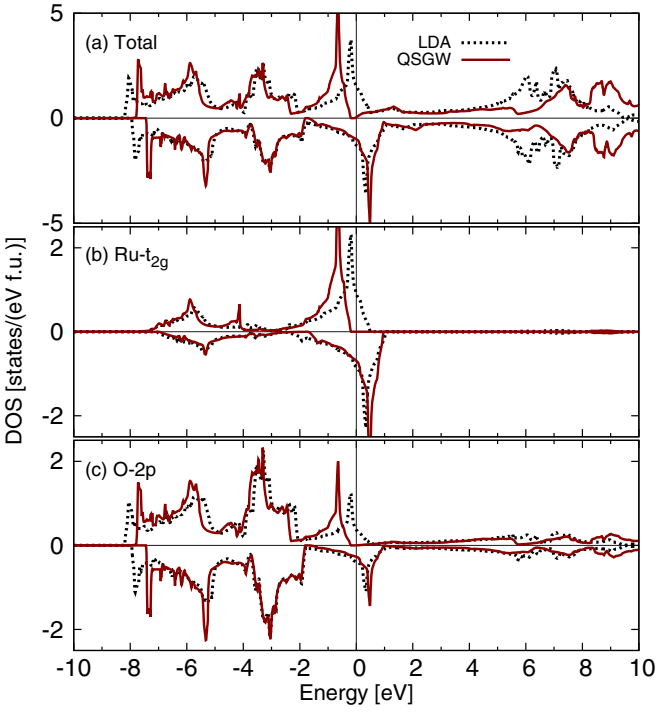

FIG. 7. The calculated (a) total DOS and (b), (c) PDOS of cubic SRO113 by LDA (black dotted lines) and QSGW (red solid lines). The Fermi level is set to zero. The positive and negative DOS represent the up- and down-spin parts, respectively.

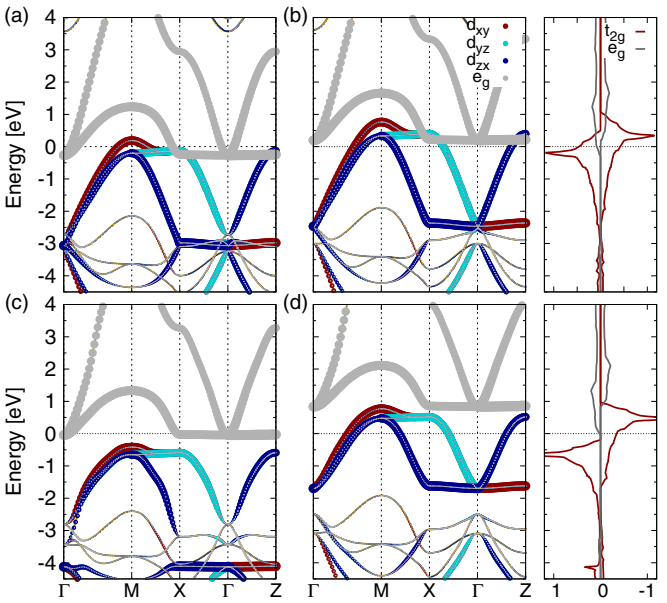

FIG. 8. The calculated band dispersion and the Ru d orbital PDOS for cubic SRO113 by (a) the LDA majority-spin band, (b) the LDA minority-spin band, (c) QSGW majority-spin band, and (d) QSGW minority-spin band. The red, cyan, blue, and gray lines refer to Ru d_{xy}, d_{yz}, d_{zx}, and e_g states, respectively. The yellow lines represent the O and Sr states (not shown in DOS). The thickness of the bands corresponds to the amount of the corresponding orbital character. The Fermi level is set to zero.

Several distinctive features are found in the QSGW results. First, notable bandwidth reduction is observed (see Figs. 7 and 8). The majority-spin bandwidth is reduced by $\sim$0.7 eV [from $\sim$3.2 eV (LDA) to $\sim$2.5 eV (QSGW)] and the minority-spin bandwidth is by $\sim$0.6 eV [from $\sim$3.2 eV (LDA) to $\sim$2.6 eV (QSGW)]. The exchange splitting is enhanced to be $\sim$1.2 eV which is significantly larger than the LDA value of $\sim$0.5 eV. We found that the naive comparison of the effective mass for LDA and QSGW based on the **k**-derivative can be misleading in SRO113 due to the different Fermi wave vectors caused by the enhanced exchange splitting in QSGW. The calculated $Z^{-1}_{\rm QSGW}$ for the up and down spin is 1.33 and 1.68, respectively. The effective mass of $m_{\rm QSGW}/m_{\rm LDA} = 1.26$ estimated from the bandwidth ratio compares reasonably well with some of DMFT results while the DMFT values show significant deviations ranging from 1.1 to 4.5 [59,88,91,92]. The specific-heat measurements report the mass enhancement of $m^*/m_{\rm LDA} = 3.7$ [50] and 4.5 [61]. The discrepancy reflects not only the limitation of RPA-QSGW correlations but also the effect of orthorhombic distortion [3,64,93].

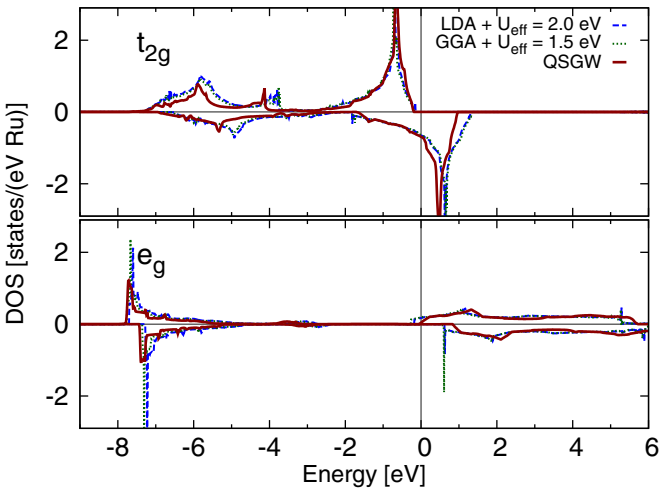

FIG. 9. The calculated Ru t_{2g} and e_g PDOS of cubic SRO113 by LDA + U ($U_{\rm eff}$ = 2.5 eV; blue dashed lines), GGA + U ($U_{\rm eff}$ = 2.0 eV; green dotted lines) and QSGW (red solid lines). The Fermi level is set to zero. The positive and negative DOS represent the up- and down-spin parts, respectively.

Together with the bandwidth reduction and the enhanced exchange splitting, the QSGW electronic structure becomes half-metallic with a gap in the majority-spin state. Note that this QSGW band structure is quite similar with DFT + U results [16,17], as shown in Fig. 9. The calculated magnetic moment of QSGW is $\mu = 2.0\mu_{\rm B}$/f.u., which is significantly larger than the LDA value and comparable with the DFT + U results [15–17]. While we only considered the cubic structure, the effect of orthorhombic distortion is basically to enhance the on-site correlations as reported by the previous study [64,93]. The experimental verification of the half-metallicity may not be easy because of the large magnetic fields required to overcome the magnetic anisotropy [56]. This possibility in SRO113 has been actively discussed based on DFT + U calculations [16,17] and hybrid functional [56]. Therefore our QSGW result adds a new promising aspect in this direction.

The detailed comparison with the DFT + U result is given in Fig. 9. The optimized values of $U_{\rm eff}$ are favorably compared with a recent constrained RPA result of $U_{\rm eff}$ = 2.1 eV although it is calculated from the orthorhombic structure [17]. For comparison one can recall that SIC-LDA result is reproduced by $U_{\rm eff}$ = 1 eV in the case of the orthorhombic structure of SRO113 [15]. As for the DMFT calculations, several different choices of U and J have been made, as in the case of SRO214. In terms of $U_{\rm eff} = U - J$, it ranges from 1.75 to 2.4 eV [59,88,91].

Several photoemission spectroscopy (PES) experiments report the LHB-like feature at ~ -2 eV [60,61,64]. The PES spectrum of orthorhombic phase [64] is plotted along with the DOS calculated by the LDA, LDA + DMFT [88], and QSGW in Fig. 5(b). The LHB-like peak near −1.5 eV is observed in the PES spectra, while not in the LDA and QSGW. It has been argued that this LHB-like feature is not related to the magnetic fluctuations or the orthorhombic structural distortion [64]. LDA + DMFT calculation of orthorhombic SRO113 with U = 3.5 and J = 1.75 eV predicts the LHB at −3 to −1 eV [88] [Fig. 5(b)]. As in SRO214, LHB is the characteristic feature of DMFT distinctive from QSGW (also from DFT + U) while some DMFT results do not seem to support this feature [59]. The absence of this state in QSGW and DFT + U (see t_{2g} states of Fig. 9) indicates that it is related to the dynamic aspects of Ru 4d correlation hybridized with O 2p as in the case of the Zhang–Rice band in cuprates. Also, regarding the half-metallic band structure, DMFT calculations do not seem to give a consistent prediction [88,92]. These issues that is likely related to the intrinsic parameter dependency require further investigations.

IV. SUMMARY

By using QSGW calculations, we re-investigated the electronic structure of SRO214 and SRO113. Without any *ad hoc* parameter or the ambiguity related to the double-counting and downfolding issues, some of the important features of electron correlations were reasonably well captured such as the bandwidth renormalization and the exchange splitting. In the case of SRO113, the QSGW result is in good agreement with the result of DFT + U over a reasonable range of the U and J parameters. While the QSGW shows limitations in describing the detailed features such as the Ru 4d spectral-weight transfer to LHB, it can be improved in combination with other techniques, as reported in recent studies [86,94,95]. Our result sheds new light on the possibility and the limitation of the first-principles electronic structure calculations of the moderately correlated transition-metal-oxide systems.

ACKNOWLEDGMENTS

S.R., S.W.J., and M.J.H. were supported by the Basic Science Research Program through the National Research Foundation of Korea (NRF) (2014R1A1A2057202; Ministry of Education) and by Samsung Advanced Institute of Technology (SAIT). The computing resource is supported by National Institute of Supercomputing and Networking / Korea Institute of Science and Technology Information with supercomputing resources including technical support (KSC-2013-C2-024) and by Computing System for Research in Kyushu University. T.K. was supported by the Advanced Low Carbon Technology Research and Development Program (ALCA), the High-efficiency Energy Conversion by Spinodal Nanodecomposition program of the Japan Science and Technology Agency (JST), and the JSPS Core-to-Core Program Advanced Research Networks ("Computational Nanomaterials Design on Green Energy").

[1] Y. Maeno, H. Hashimoto, K. Yoshida, S. Nishizaki, T. Fujita, J. G. Bednorz, and F. Lichtenberg, Nature (London) **372**, 532 (1994); G. M. Luke, Y. Fudamoto, K. M. Kojima, M. I. Larkin, J. Merrin, B. Nachumi, Y. J. Uemura, Y. Maeno, Z. Q. Mao, Y. Mori, H. Nakamura, and M. Sigrist, *ibid.* **394**, 558 (1998); K. Ishida, H. Mukuda, Y. Kitaoka, K. Asayama, Z. Q. Mao, Y.

Mori, and Y. Maeno, *ibid.* **396**, 658 (1998); T. M. Rice and M. Sigrist, J. Phys.: Condens. Matter **7**, L643 (1995); G. Baskaran, Phys. B (Amsterdam, Neth.) **223–224**, 490 (1996).
[2] J. Mravlje, M. Aichhorn, T. Miyake, K. Haule, G. Kotliar, and A. Georges, Phys. Rev. Lett. **106**, 096401 (2011).
[3] A. Georges, L. de' Medici, and J. Mravlje, Annu. Rev. Condens. Matter Phys. **4**, 137 (2013).
[4] L. de' Medici, J. Mravlje, and A. Georges, Phys. Rev. Lett. **107**, 256401 (2011).
[5] S. B. Chung, S. Raghu, A. Kapitulnik, and S. A. Kivelson, Phys. Rev. B **86**, 064525 (2012).
[6] Q. H. Wang, C. Platt, Y. Yang, C. Honerkamp, F. C. Zhang, W. Hanke, T. M. Rice, and R. Thomale, Europhys. Lett. **104**, 17013 (2013).
[7] J.-W. Huo and F.-C. Zhang, Phys. Rev. B **87**, 134501 (2013).
[8] C. Rastovski, C. D. Dewhurst, W. J. Gannon, D. C. Peets, H. Takatsu, Y. Maeno, M. Ichioka, K. Machida, and M. R. Eskildsen, Phys. Rev. Lett. **111**, 087003 (2013).
[9] T. Scaffidi, J. C. Romers, and S. H. Simon, Phys. Rev. B **89**, 220510(R) (2014).
[10] A. Callaghan, C. W. Moeller, and R. Ward, Inorg. Chem. (Washington, DC, U. S.) **5**, 1572 (1966).
[11] J. J. Neumeier, A. L. Cornelius, and J. S. Schilling, Phys. B (Amsterdam, Neth.) **198**, 324 (1994).
[12] A. Kanbayasi, J. Phys. Soc. Jpn. **41**, 1876 (1976).
[13] J. M. Longo, P. M. Raccah, and J. B. Goodenough, J. Appl. Phys. **39**, 1327 (1968).
[14] G. Cao, S. McCall, M. Shepard, J. E. Crow, and R. P. Guertin, Phys. Rev. B **56**, 321 (1997).
[15] J. M. Rondinelli, N. M. Caffrey, S. Sanvito, and N. A. Spaldin, Phys. Rev. B **78**, 155107 (2008).
[16] H.-T. Jeng, S.-H. Lin, and C.-S. Hsue, Phys. Rev. Lett. **97**, 067002 (2006).
[17] P. Mahadevan, F. Aryasetiawan, A. Janotti, and T. Sasaki, Phys. Rev. B **80**, 035106 (2009).
[18] F. Le Marrec, A. Demuer, D. Jaccard, J.-M. Triscone, M. K. Lee, and C. B. Eom, Appl. Phys. Lett. **80**, 2338 (2002).
[19] K. S. Takahashi, A. Sawa, Y. Ishii, H. Akoh, M. Kawasaki, and Y. Tokura, Phys. Rev. B **67**, 094413 (2003).
[20] H. N. Lee, H. M. Christen, M. F. Chisholm, C. M. Rouleau, and D. H. Lowndes, Appl. Phys. Lett. **84**, 4107 (2004).
[21] C. H. Ahn, T. Tybell, L. Antognazza, K. Char, R. H. Hammond, M. R. Beasley, Ø. Fischer, and J.-M. Triscone, Science **276**, 1100 (1997).
[22] K. S. Takahashi, M. Gabay, D. Jaccard, K. Shibuya, T. Ohnishi, M. Lippmaa, and J.-M. Triscone, Nature (London) **441**, 195 (2006).
[23] C. H. Ahn, R. H. Hammond, T. H. Geballe, M. R. Beasley, J.-M. Triscone, M. Decroux, Ø. Fischer, L. Antognazza, and K. Char, Appl. Phys. Lett. **70**, 206 (1997).
[24] T. Oguchi, Phys. Rev. B **51**, 1385 (1995).
[25] D. J. Singh, Phys. Rev. B **52**, 1358 (1995).
[26] I. Hase and Y. Nishihara, J. Phys. Soc. Jpn. **65**, 3957 (1996).
[27] G. J. McMullan, M. P. Ray, and R. J. Needs, Phys. B (Amsterdam, Neth.) **223–224**, 529 (1996).
[28] C. Noce and M. Cuoco, Phys. Rev. B **59**, 2659 (1999).
[29] A. P. Mackenzie, S. Ikeda, Y. Maeno, T. Fujita, S. R. Julian, and G. G. Lonzarich, J. Phys. Soc. Jpn. **67**, 385 (1998).
[30] A. P. Mackenzie, S. R. Julian, A. J. Diver, G. J. McMullan, M. P. Ray, G. G. Lonzarich, Y. Maeno, S. Nishizaki, and T. Fujita, Phys. Rev. Lett. **76**, 3786 (1996).
[31] C. Bergemann, S. R. Julian, A. P. Mackenzie, S. NishiZaki, and Y. Maeno, Phys. Rev. Lett. **84**, 2662 (2000).
[32] D. H. Lu, M. Schmidt, T. R. Cummins, S. Schuppler, F. Lichtenberg, and J. G. Bednorz, Phys. Rev. Lett. **76**, 4845 (1996).
[33] T. Yokoya, A. Chainani, T. Takahashi, H. Ding, J. C. Campuzano, H. Katayama-Yoshida, M. Kasai, and Y. Tokura, Phys. Rev. B **54**, 13311 (1996).
[34] A. Damascelli, D. H. Lu, K. M. Shen, N. P. Armitage, F. Ronning, D. L. Feng, C. Kim, Z.-X. Shen, T. Kimura, Y. Tokura, Z. Q. Mao, and Y. Maeno, Phys. Rev. Lett. **85**, 5194 (2000).
[35] R. Matzdorf, Z. Fang, Ismail, Jiandi Zhang, T. Kimura, Y. Tokura, K. Terakura, and E. W. Plummer, Science **289**, 746 (2000).
[36] K. M. Shen, A. Damascelli, D. H. Lu, N. P. Armitage, F. Ronning, D. L. Feng, C. Kim, Z.-X. Shen, D. J. Singh, I. I. Mazin, S. Nakatsuji, Z. Q. Mao, Y. Maeno, T. Kimura, and Y. Tokura, Phys. Rev. B **64**, 180502(R) (2001).
[37] D. J. Singh, Phys. Rev. B **77**, 046101 (2008).
[38] Z. V. Pchelkina, I. A. Nekrasov, Th. Pruschke, S. Suga, V. I. Anisimov, and D. Vollhardt, Phys. Rev. B **77**, 046102 (2008).
[39] T. Yokoya, A. Chainani, T. Takahashi, H. Katayama-Yoshida, M. Kasai, Y. Tokura, N. Shanthi, and D. D. Sarma, Phys. Rev. B **53**, 8151 (1996).
[40] I. H. Inoue, Y. Aiura, Y. Nishihara, Y. Haruyama, S. Nishizaki, Y. Maeno, Y. Fujita, J. G. Bednorz, and F. Lichtenberg, Phys. B (Amsterdam, Neth.) **223–224**, 516 (1996).
[41] I. H. Inoue, A. Kimura, A. Harasawa, A. Kakizaki, Y. Aiura, S. Ikeda, and Y. Maeno, J. Phys. Chem. Solids **59**, 2205 (1998).
[42] T. T. Tran, T. Mizokawa, S. Nakatsuji, H. Fukazawa, and Y. Maeno, Phys. Rev. B **70**, 153106 (2004).
[43] C. Bergemann, A. P. Mackenzie, S. R. Julian, D. Forsythe, and E. Ohmichi, Adv. Phys. **52**, 639 (2003).
[44] H. Iwasawa, Y. Aiura, T. Saitoh, I. Hase, S. I. Ikeda, Y. Yoshida, H. Bando, M. Higashiguchi, Y. Miura, X. Y. Cui, K. Shimada, H. Namatame, and M. Taniguchi, Phys. Rev. B **72**, 104514 (2005).
[45] A. V. Puchkov, Z.-X. Shen, T. Kimura, and Y. Tokura, Phys. Rev. B **58**, R13322 (1998).
[46] A. Pérez-Navarro, J. Costa-Quintana, and F. López-Aguilar, Phys. Rev. B **61**, 10125 (2000).
[47] A. Liebsch and A. Lichtenstein, Phys. Rev. Lett. **84**, 1591 (2000).
[48] Z. V. Pchelkina, I. A. Nekrasov, Th. Pruschke, A. Sekiyama, S. Suga, V. I. Anisimov, and D. Vollhardt, Phys. Rev. B **75**, 035122 (2007).
[49] V. I. Anisimov, F. Aryasetiawan, and A. I. Lichtenstein, J. Phys.: Condens. Matter **9**, 767 (1997); G. Kotliar, S. Y. Savrasov, K. Haule, V. S. Oudovenko, O. Parcollet, and C. A. Marianetti, Rev. Mod. Phys. **78**, 865 (2006).
[50] P. B. Allen, H. Berger, O. Chauvet, L. Forro, T. Jarlborg, A. Junod, B. Revaz, and G. Santi, Phys. Rev. B **53**, 4393 (1996).
[51] G. Santi and T. Jarlborg, J. Phys.: Condens. Matter **9**, 9563 (1997).
[52] I. I. Mazin and D. J. Singh, Phys. Rev. B **56**, 2556 (1997).
[53] Y. J. Chang, C. H. Kim, S.-H. Phark, Y. S. Kim, J. Yu, and T. W. Noh, Phys. Rev. Lett. **103**, 057201 (2009).
[54] J. Xia, W. Siemons, G. Koster, M. R. Beasley, and A. Kapitulnik, Phys. Rev. B **79**, 140407(R) (2009).

[55] K. Gupta, B. Mandal, and P. Mahadevan, Phys. Rev. B **90**, 125109 (2014).

[56] M. Verissimo-Alves, P. García-Fernández, D. I. Bilc, P. Ghosez, and J. Junquera, Phys. Rev. Lett. **108**, 107003 (2012).

[57] L. Si, Z. Zhong, J. M. Tomczak, and K. Held, Phys. Rev. B **92**, 041108(R) (2015).

[58] P. Werner, E. Gull, M. Troyer, and A. J. Millis, Phys. Rev. Lett. **101**, 166405 (2008).

[59] H. T. Dang, J. Mravlje, A. Georges, and A. J. Millis, Phys. Rev. B **91**, 195149 (2015).

[60] K. Fujioka, J. Okamoto, T. Mizokawa, A. Fujimori, I. Hase, M. Abbate, H. J. Lin, C. T. Chen, Y. Takeda, and M. Takano, Phys. Rev. B **56**, 6380 (1997).

[61] J. Okamoto, T. Mizokawa, A. Fujimori, I Hase, M. Nohara, H. Takagi, Y. Takeda, and M. Takano, Phys. Rev. B **60**, 2281 (1999).

[62] H.-D. Kim, H.-J. Noh, K. H. Kim, and S.-J. Oh, Phys. Rev. Lett. **93**, 126404 (2004); J. Park, S.-J. Oh, J.-H. Park, D. M. Kim, and C.-B. Eom, Phys. Rev. B **69**, 085108 (2004); W. Siemons, G. Koster, A. Vailionis, H. Yamamoto, D. H. A. Blank, and M. R. Beasley, *ibid.* **76**, 075126 (2007); E. B. Guedes, M. Abbate, K. Ishigami, A. Fujimori, K. Yoshimatsu, H. Kumigashira, M. Oshima, F. C. Vicentin, P. T. Fonseca, and R. J. O. Mossanek, *ibid.* **86**, 235127 (2012).

[63] K. Maiti and R. S. Singh, Phys. Rev. B **71**, 161102(R) (2005).

[64] M. Takizawa, D. Toyota, H. Wadati, A. Chikamatsu, H. Kumigashira, A. Fujimori, M. Oshima, Z. Fang, M. Lippmaa, M. Kawasaki, and H. Koinuma, Phys. Rev. B **72**, 060404(R) (2005).

[65] S. V. Faleev, M. van Schilfgaarde, and T. Kotani, Phys. Rev. Lett. **93**, 126406 (2004).

[66] M. van Schilfgaarde, T. Kotani, and S. Faleev, Phys. Rev. Lett. **96**, 226402 (2006).

[67] T. Kotani, M. van Schilfgaarde, and S. V. Faleev, Phys. Rev. B **76**, 165106 (2007).

[68] J. Kliměš, M. Kaltak, and G. Kresse, Phys. Rev. B **90**, 075125 (2014).

[69] F. Bruneval, J. Chem. Phys. **136**, 194107 (2012).

[70] R. Shaltaf, G.-M. Rignanese, X. Gonze, F. Giustino, and A. Pasquarello, Phys. Rev. Lett. **100**, 186401 (2008).

[71] W. R. L. Lambrecht, Phys. Status Solidi B **248**, 1547 (2011).

[72] T. Kotani and M. van Schilfgaarde, J. Phys.: Condens. Matter **20**, 295214 (2008).

[73] M. J. Han, H. Kino, and T. Kotani, Phys. Rev. B **90**, 035127 (2014).

[74] S. W. Jang, T. Kotani, H. Kino, K. Kuroki, and M. J. Han, Sci. Rep. **5**, 12050 (2015).

[75] A. N. Chantis, M. van Schilfgaarde, and T. Kotani, Phys. Rev. B **76**, 165126 (2007).

[76] The electronic structure simulation package, ECALJ implemented by T. Kotani, https://github.com/tkotani/ecalj; LMTO electronic structure simulation package, LM SUITE. http://www.lmsuite.org

[77] T. Kotani, J. Phys. Soc. Jpn. **83**, 094711 (2014); T. Kotani and M. van Schilfgaarde, Phys. Rev. B **81**, 125117 (2010); T. Kotani and H. Kino, J. Phys. Soc. Jpn. **82**, 124714 (2013); T. Kotani, H. Kino, and H. Akai, *ibid.* **84**, 034702 (2015).

[78] B. C. Chakoumakos, S. E. Nagler, S. T. Misture, and H. M. Christen, Phys. B (Amsterdam, Neth.) **241–243**, 358 (1998).

[79] It is found that the inclusion of the M point $(\pi,0,0)$ is important due to the existence of Van Hove singularity. As a result, the result of $7 \times 7 \times 7$ **k** points shows the unusually large deviation from the $6 \times 6 \times 6$ result. Due to the large computation cost, we could not further increase the number of **k** points.

[80] T. Ozaki, Phys. Rev. B **67**, 155108 (2003).

[81] J. P. Perdew and A. Zunger, Phys. Rev. B **23**, 5048 (1981).

[82] J. P. Perdew, K. Burke, and M. Ernzerhof, Phys. Rev. Lett. **77**, 3865 (1996).

[83] S. L. Dudarev, G. A. Botton, S. Y. Savrasov, C. J. Humphreys, and A. P. Sutton, Phys. Rev. B **57**, 1505 (1998).

[84] M. J. Han, T. Ozaki, and J. Yu, Phys. Rev. B **73**, 045110 (2006).

[85] There is no significant difference between the DOS and $A(\omega)$ obtained by QSGW [see Fig. 2(e)]. Therefore, our discussion below will mainly be based on DOS.

[86] J. M. Tomczak, M. Casula, T. Miyake, and S. Biermann, Phys. Rev. B **90**, 165138 (2014).

[87] H. Iwasawa, Y. Yoshida, I. Hase, S. Koikegami, H. Hayashi, J. Jiang, K. Shimada, H. Namatame, M. Taniguchi, and Y. Aiura, Phys. Rev. Lett. **105**, 226406 (2010).

[88] E. Jakobi, S. Kanungo, S. Sarkar, S. Schmitt, and T. Saha-Dasgupta, Phys. Rev. B **83**, 041103(R) (2011).

[89] M. W. Haverkort, I. S. Elfimov, L. H. Tjeng, G. A. Sawatzky, and A. Damascelli, Phys. Rev. Lett. **101**, 026406 (2008).

[90] We estimated Z^{-1}_{QSGW} at the Γ point.

[91] O. Grånäs, I. Di Marco, O. Eriksson, L. Nordström, and C. Etz, Phys. Rev. B **90**, 165130 (2014).

[92] M. Kim and B. I. Min, Phys. Rev. B **91**, 205116 (2015).

[93] E. Pavarini, S. Biermann, A. Poteryaev, A. I. Lichtenstein, A. Georges, and O. K. Andersen, Phys. Rev. Lett. **92**, 176403 (2004).

[94] J. M. Tomczak, M. van Schilfgaarde, and G. Kotliar, Phys. Rev. Lett. **109**, 237010 (2012).

[95] S. Choi, A. Kutepov, K. Haule, M. van Schilfgaarde, and G. Kotliar, arXiv:1504.07569.